Volume 1 | Number 1 | Jan 2013 | Pages 1–100

Nanoscale

www.rsc.org/nanoscale

ROYAL SOCIETY OF CHEMISTRY

This is an *Accepted Manuscript*, which has been through the Royal Society of Chemistry peer review process and has been accepted for publication.

Accepted Manuscripts are published online shortly after acceptance, before technical editing, formatting and proof reading. Using this free service, authors can make their results available to the community, in citable form, before we publish the edited article. We will replace this *Accepted Manuscript* with the edited and formatted *Advance Article* as soon as it is available.

You can find more information about *Accepted Manuscripts* in the **Information for Authors**.

ROYAL SOCIETY OF CHEMISTRY

www.rsc.org/nanoscale

Nanoscale

COMMUNICATION

Graphene nanoarchitecture in batteries

Di Wei [a*], Michael R. Astley [a], Nadine Harris [a], Richard White [a], Tapani Ryhänen [a] and Jani Kivioja [a]

We compare three different carbon nanoarchitectures used to produce standard coin cell batteries: graphene monolayer, graphite paper and graphene foam. The batteries' electrochemical performances are characterised using cyclic voltammerty, constant-current discharge and dynamic galvanostatic techniques. Even though graphene is the fundamental building block of graphite its properties are intrinsically different when used in batteries because there is no ion intercalation in graphene. The nanoarchitecture of the graphene electrode is shown to have a strong influence over the battery's electrochemical performance. This provides a versatile way to design various battery electrodes on different demands.

Traditionally bulk graphite is used in lithium metal batteries (LBs) and lithium ion batteries (LIBs) because it affords high energy density. One of the reasons graphite has become the industry standard material is because of its effective Li+ ion intercalation properties [1], [2], where Li+ ions are inserted between the graphene layers. However, this has the drawback of causing slow, diffusion limited, recharging times because a reverse voltage is needed to remove the Li+ ions from the graphite and force them back from the cathode to the anode via the electrolyte.

An increasing amount of research has focussed on improving the energy density and power density of LBs/LIBs by replacing the graphite with different carbon materials, such as carbon nanotubes, fullerenes and graphene-based materials [3], [4]. These 'graphenes' are mostly either multi-layer graphenes or reduced graphene oxides containing defects and contaminants, and not possessing some of the intrinsic physical properties of pristine graphene that can be made with the chemical vapour

deposition (CVD) method. Recently we have shown that CVD-grown monolayer graphene can work as a LB electrode [5]. Even though as building block of graphite [6], perfect graphene as monolayer has many unique properties that graphite does not possess, like quantum capacitance. Also, it has been reported that charge flows at higher speeds in such two-dimensional (2D) nanoflakes than in bulk compounds [7], [8]. Graphene conducts electricity even better than theory predicts on steps etched in silicon carbide [8].

Reports describe repulsive Coulombic forces between Li+ at the graphene electrode [9] as well as an inability for Li+ to intercalate or absorb strongly to the surface of defect-free graphene [10]. Jang et al. [11] recently developed a combined high power (100 kW/kgcell) and high energy density device (160 Wh/kgcell) based on porous electrodes with large amounts of graphene surfaces in direct contact with the electrolyte. The use of graphene, as opposed to graphite, allowed the Li+ to reach the interior graphene surfaces without the need to undergo intercalation. After recharging, via an external source, enormous fluxes of Li+ ions were quickly released from the cathode to the anode and re-established the initial electrochemical potential.

Despite numerous publications about different carbon materials and structures including the ultrathin graphite foam structures [12], there have been few attempts to directly compare different graphene nanoarchitectures in a systematic manner. In this manuscript we have examined three different carbon nano-architectures: monolayer graphene, graphite paper (stacked multi-layered graphene) and graphene foam (monolayer graphene grown on a microporous Cu foam substrate).

The monolayer graphene sample was commercially bought from Graphenea Ltd., and detailed results from this sample have been reported previously [5]. Briefly, the monolayer graphene film was grown by chemical vapour

deposition (CVD) on top of a copper foil substrate in an Aixtron CVD reactor. After growth, characterisation by Raman spectroscopy, transmission electron microscopy and selected area electron diffraction confirmed the defect-free monolayer nature of the graphene.

Graphene coated on Cu foam was purchased from Graphene supermarket. A copper foam template is used as the substrate to grow graphene by a similar CVD process to the monolayer graphene sample. Graphene on Cu foam can be considered as a three-dimensional scaled-up version of monolayer graphene on Cu foil.

Graphite paper was purchased from SIGRAFLEX® of SGL Group; it was manufactured from expanded natural graphite, a homogeneous material without adhesives or binders. This prevents any electrochemical influence from chemical additives affecting the results.

The different carbon materials were used to construct standard 2032 coin-cell batteries [Fig. 1(a)]. The monolayer graphene on Cu-foil / graphene on Cu foam / graphite paper was used directly as the working electrode (cathode) with the Li-foil as the counter electrode (anode). The polymer electrolyte acts as a separator between the anode and cathode and is composed of a poly(ethylene glycol) borate ester, which enhances Li+ transport and makes it comparable with conventional liquid organic electrolytes at room temperature [13]. Additionally the polymer electrolyte was wetted by 1M solution of $LiPF_6$ in a 1:1 (v/v) mixture of ethylene carbonate and diethyl carbonate. The coin-cells were assembled within an MBraun glovebox (H2O < 0.1ppm, O2 < 0.1ppm) filled with inert Ar gas.
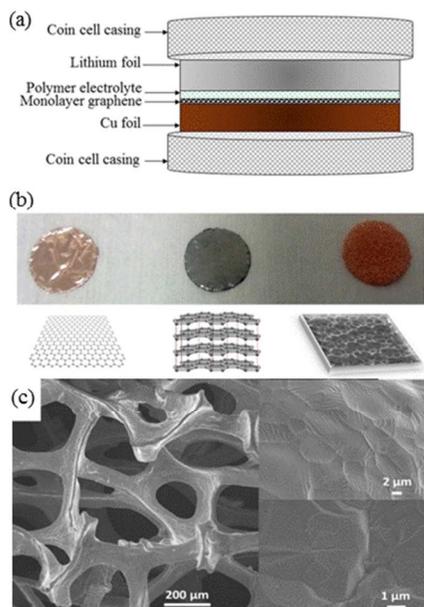
Fig 1 (a) Cross-sectional view of fabricated coin-cell device with monolayer graphene battery electrode; (b) electrodes made from monolayer graphene on Cu foil (left), graphite paper (centre) and CVD graphene on Cu foam (right); (c) scanning electron micrograph of CVD graphene on Cu foam

The advantages of using the coin-cell structure are twofold: firstly the direct electrochemistry of graphene may be studied without the need to transfer the graphene from Cu to other substrates; and secondly the electrochemical influence of Cu is negated due to the graphene layer. It should be noted that our graphene batteries are classed as Li-metal batteries as opposed to a conventional LIB, where the anode is comprised of graphite.

The electrochemical properties of the assembled coin-cell were studied with a Maccor battery tester and Autolab while cyclic voltammogram measurements were taken with Autolab. The following results have been repeated on multiple battery samples, with similar behaviour observed throughout. Additionally, parallel experiments using pure Cu foil (without graphene or graphite) showed no open circuit voltage, confirming that the graphene/graphite is responsible for these results.

Cyclic voltammetry (CV) measurements were used to examine the Li+ interactions with the graphene surface. Three CV cycles between 0V and 3V (measured versus the Li anode) at a scan rate of 0.1mV/s are shown in Fig. 2.
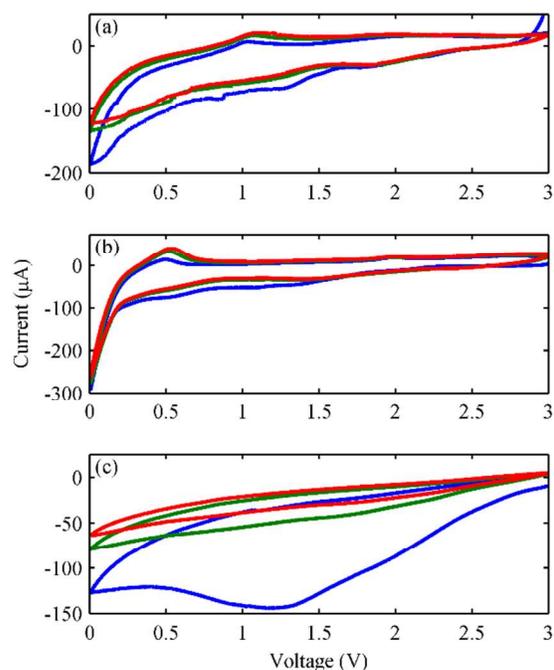
Fig. 2 CV measurements between 0V and 3V (measured versus the anode). First (blue), second (green) and third (red) cycles are shown for batteries made using (a) monolayer graphene, (b) graphite paper and (c) graphene foam

Due to the formation of the solid electrolyte interface (SEI) layer, the current density of the first cycle is largest when compared with the second and third cycles, which is also apparent when monolayer graphene is chemically modified [14]. The cathodic peak at ~1.0V in Fig. 2(a) has been observed previously in monolayer graphene on Cu in polymer electrolyte [9].

In conventional LIBs the intercalation of Li+ into graphite causes the appearance of well-defined peaks from 0V to ~0.5V [5], [9]. There are no obvious peaks below 0.5V for the three CV cycles shown in Fig. 2(a) confirming that there is no intercalation of Li+ in the monolayer graphene [11]. By way of contrast, Fig. 2(b) shows very sharp Li+ insertion and extraction peaks at ~0V and ~0.5V respectively, showing that intercalation occurs in the graphite paper. The graphene on Cu foam sample (Fig. 2(c)) does not show peaks from Li+

intercalation near 0V, indicating that the coating on the Cu foam is indeed mono/few layer.

Intercalation of Li+ ions has a detrimental effect on the structural integrity of the electrode. We observed this directly by the level of degradation suffered by the graphite paper battery during long-term discharge tests (supplementary Fig. 1). The monolayer graphene and graphene foam batteries showed no such degradation, consistent with the CV observations that no Li+ intercalation takes place in graphene.

Discharge curves for the batteries are presented in Fig. 3. The batteries were discharged with a 0.5mA load current until 0V output voltage was reached. Open circuit potentials of ~2.25V for the three cells are similar to other carbon based materials such as carbon nanotubes and pristine graphene etc.[3], [4] In Fig. 3, a plateau below 1.2V that correlates with the formation of an SEI film was observed in all three batteries [15]. The continuous voltage drop observed from 0.8V until the end of discharge at 0.01V has been ascribed to the 'space charge' region [16]. For the size of standard 2032 coin cell (2cm diameter), the energy capacity at first discharge cycle for the monolayer graphene is about 0.009mAh, for graphite paper is about 0.06mAh and for graphene foam is about 1.55mAh.
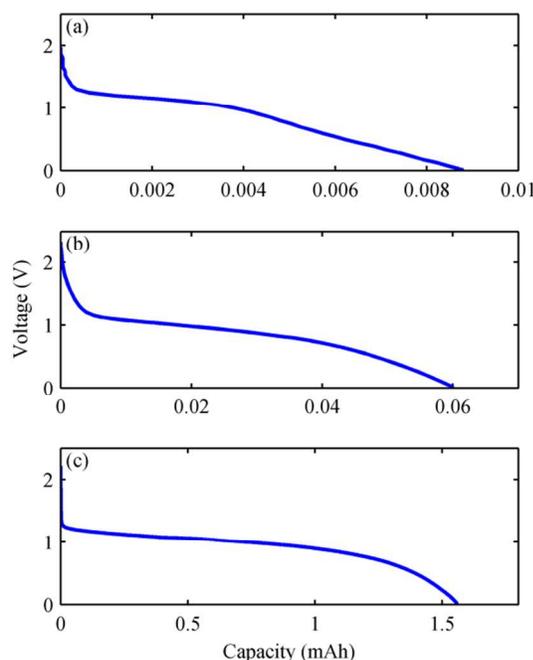
Fig. 3 First discharge curve under current of 0.5mA for batteries made using (a) monolayer graphene, (b) graphite paper and (c) graphene foam

After the first discharge shown in Fig. 3 the discharge current was reduced to 0A for 5 minutes, then the battery was recharged with a 0.5mA current until 3V. Voltages recovered gradually after the discharge and once the charging current of 0.5mA was applied the voltage immediately reaches 3V. As supplementary Fig. 2 shows, the energy capacities drop in the forthcoming cycles for all three cells. After 10 times discharge charge cycles at a current of 0.5mA, the energy capacity for battery made from monolayer graphene drops to 0.001mAh, graphite paper to 0.005mAh and graphene foam to 0.012mAh.

The dynamic properties of the batteries were further studied using galvanostatic measurements. The batteries were repeatedly

discharged under a constant current (I_{load}) for 2 seconds and then allowed to recover for 30 seconds at 0A. In Fig. 4 the results of four discharge/recovery cycles are presented, taken with load currents of 100μA, 250μA and 500μA. In all cases a substantial recovery of the battery voltage occurs during the recovery period. It should be noticed that the gravimetric current value (A/g) applied on graphene electrode is actually much higher than that applied on graphite considering the huge mass difference (supplementary). However, we can still see stable energy capacities for graphene based electrodes, which indicates graphene based electrodes have much higher discharge-rate.
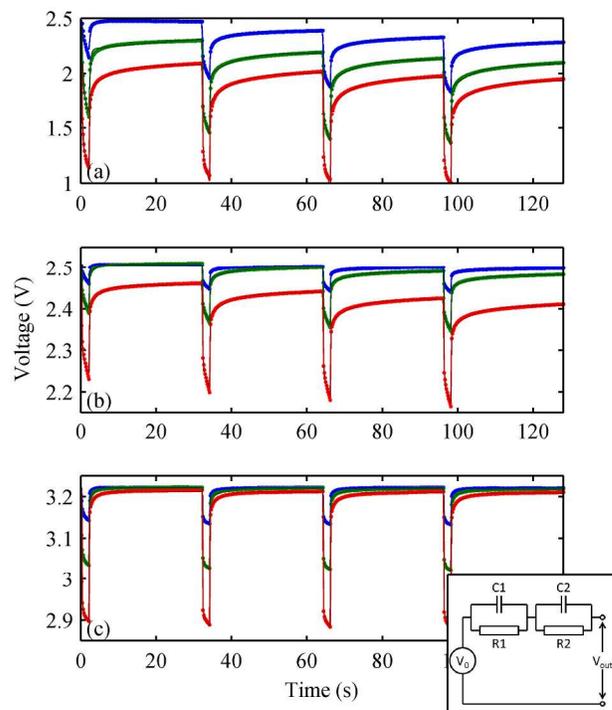
Fig. 4 Galvanostatic discharge/recover results for batteries made using (a) monolayer graphene, (b) graphite paper and (c) graphene foam; 100μA (blue), 250μA (green) and 500μA (red) discharge currents; circles show experimental data points, solid lines show model fits. Inset: schematic of the equivalent circuit model

The discharge/recovery cycle features a clear double-exponential decay. A heuristic equivalent circuit model was developed to describe this behaviour featuring two RC elements (inset of Fig 4); we note that this model shows strong similarities with the double-polarisation model developed by He *et al.* to describe LIBs [17]. The battery output voltage (V_{out}) is defined by the coupled equations:

$$V_{out} = V_0 - V_1 - V_2$$
$$C_1 \frac{dV_1}{dt} = I_{load} - \frac{V_1}{R_1}$$
$$C_2 \frac{dV_2}{dt} = I_{load} - \frac{V_2}{R_2}$$

To fit the model parameters V_0, R_1, R_2, C_1 and C_2, the values of these parameters were assumed to remain constant over a single discharge/recovery cycle, but allowed to change over

COMMUNICATION

subsequent cycles. V_0 is the open circuit voltage and R_1, R_2, C_1 and C_2 are series impedance elements in the battery. Trial discharge/recovery cycle curves were calculated by solving the above equations numerically, and an iterative least squares non-linear regression algorithm was used to fit the model to the experimental data (using the MATLAB *nlinfit* function). As shown in Fig. 4, such macroscopic double-polarisation equivalent circuit can well-describe the experimentally observed battery-discharge phenomenon. However, the underlying physics of this dynamic, non-equilibrium system is far from straightforward: the free lithium ions, polymer electrolyte, semiconducting graphene and copper substrate are all interacting elements and cannot be treated independently. Even though we can not assign specific physical meaning to parameters such as C_1 and C_2, macroscopic models that represent complicated underlying physical processes in simple terms are incredibly useful to create meaningful comparisons.

The model fit to the second, third and fourth discharge/recovery cycles was excellent (the initial cycle fit was typically of much worse quality) - average model parameters extracted from the fitting are shown in supplementary table 1. The values of capacitance etc. discussed in the following are corresponding to these discharge/charge cycles. While the model has been derived heuristically, we note that the relatively large capacitance values (as large as $\sim 5\,\mathrm{mFcm^{-2}}$ for graphene foam) are correlated with the formation of Helmholtz double-layers at the electrode/electrolyte interface [18]. Interestingly, in both the monolayer graphene battery and the graphene foam battery there is a strong dependence of C_1 on discharge current, suggesting that the distance between the Helmholtz planes, the permittivity of the intervening electrolyte or the electrochemical properties of the electrodes are changing with current flow; however, this effect is not seen in the graphite paper battery, and so is likely related to the fact that Li+ ion intercalation is suppressed at the graphene interface. It was recently reported that a monolayer graphene electrode has a very different specific surface area and area-normalized capacitance [19] than a graphite electrode. A smaller area-normalized capacitance for conventional graphite electrodes was explained by invoking a space charge capacitance, representing a spread of induced electrode charge into the bulk, in series with the Helmholtz capacitance located on the electrolyte side of interface, between the electrolyte and bulk solid. The enhanced capacitance for mono- and few-layer graphene electrodes was attributed to correlations between the π-band electron Fermi liquid and ions in the Helmholtz layer (quantum capacitance) [20]. This voltage-correlated quantum capacitance [18] may be related to the dependence of C_1 on discharge current for graphene-based electrodes; however a full understanding of how these are related requires a self-consistent thermoelectric model of the interactions between graphene, copper, lithium ions and electrolyte, which is beyond the scope of this paper.

The recovery effect behaviour seen in Fig. 3 could potentially be caused by non-zero leakage currents recharging the battery when the test equipment was set to zero load current. To confirm that this was not the case, similar discharge/recovery cycles were performed using a metal-film resistor to load the batteries, connected to the battery via a relay switch, and with the voltage monitored using a Keithley 6517A electrometer with sub-femtoamp leakage currents. The results (supplementary Fig. 3) show equivalent behaviour to the galvanostatic measurements; furthermore, the behaviour was seen to persist over several hours and many hundreds of cycles.

Conclusions

We have fabricated standard coin cell batteries which differ solely in the nanoarchitecture of the carbon used to construct the battery electrode. However we find that the electrochemical properties of these batteries are strongly determined by that carbon nanoarchitecture: CV measurements confirmed that Li+ ion intercalation is not a factor in both monolayer graphene and graphene foam electrodes, and discharge measurements demonstrated that the capacity of the battery can be greatly increased by using a foam electrode structure. Furthermore, galvanostatic measurements have shown that, while the dynamic discharge and recovery behaviour of the battery is well described by a double RC model in all cases, the parameter values (both in terms of absolute value and dependence on other variables) are dependent on the nanoarchitecture of the battery.

In summary, we have shown that graphene is different than graphite when used in battery electrodes; additionally, the energy capacity and dynamic response can be optimised by changing the graphene architecture. The electrode nanoarchitecture requires careful consideration as a fundamental material property that can strongly influence the electrochemical performance of the battery.

Acknowledgement

Notes and references

a Nokia R&D UK Ltd, Broers Building, 21 J. J. Thomson Avenue, CB3 0FA, Cambridge, UK. E-mail: di.wei@nokia.com

[1]   M. Armand and J.-M. Tarascon, *Nature*, 2008, **451**, 652.

[2]   J. R. Dahn, T. Zheng, Y. Liu, and J. S. Xue, *Science,* 2013, **270**, 590.

[3]   Z.-S. Wu, W. Ren, L. Xu, F. Li, and H.-M. Cheng, *ACS Nano*, 2011, **5**, 5463.

[4]   Y.-J Xu, X. Liu, G. Cui, B. Zhu, G. Weinberg, R. Schlogl, J. Maier, D. S. Su, *ChemSusChem*, 2010, **3**, 343.

[5]   D. Wei, S. Haque, P. Andrew, J. Kivioja, T. Ryhänen, A. Pesquera, A. Centeno, B. Alonso, A. Chuvilin, and A. Zurutuza, *J. Mater. Chem. A*, 2013, **1**, 3177.

[6]   B. Partoens and F. Peeters, *Phys. Rev. B*, 2006, **74**, 075404.

[7]   E. S. Reich, *Nature*, 2014, **506**, 19.

[8]   J. Baringhaus, M. Ruan, F. Edler, A. Tejeda, M. Sicot, A.-P. Li, Z. Jiang, E. H. Conrad, C. Berger, C. Tegenkamp, and W. A. de Heer, *Nature*, 2014, **0**, 1.

[9]   E. Pollak, B. Geng, K.-J. Jeon, I. T. Lucas, T. J. Richardson, F. Wang, and R. Kostecki, *Nano Lett.*, 2010, **10**, 3386.

[10]   E. Lee and K. A Persson, *Nano Lett.*, 2012, **12,** 4624.

[11]   B. Z. Jang, C. Liu, D. Neff, Z. Yu, M. C. Wang, W. Xiong, and A. Zhamu, *Nano Lett.*, 2011, **11,** 3785.

[12]   H. Ji, L. Zhang, M. Pettes, H. Li, S. Chen, L. Shi, R. Piner, and R. Ruoff, *Nano Lett.*, 2012, **12**, 2446.

[13]   Y. Kato, K. Hasumi, S. Yokoyama, T. Yabe, and H. Ikuta, *Solid State Ionics*, 2002, **150**, 355.

[14]   L. Gan, D. Zhang, and X. Guo, *Small*, 2012, **8**, 1326.

[15]   C. Wang, A. J. Appleby, and F. E. Little, *Electrochim. Acta*, 2001, **46**, 1793.

[16]   Y.-Y. Hu, Z. Liu, K.-W. Nam, O. J. Borkiewicz, J. Cheng, X. Hua, M. T. Dunstan, X. Yu, K. M. Wiaderek, L.-S. Du, K. W. Chapman, P. J. Chupas, X.-Q. Yang, and C. P. Grey, *Nat. Mater.*, 2013, **12**, 1130.

[17]   H. He, R. Xiong, and J. Fan, *Energies*, 2011, **4**, 582.

[18]   M. D. Stoller, C. W. Magnuson, Y. Zhu, S. Murali, J. W. Suk, R. Piner, and R. S. Ruoff, *Energy Environ. Sci.*, 2011, **4**, 4685.

[19]   H. Ji, X. Zhao, Z. Qiao, J. Jung, Y. Zhu, Y. Lu, L. L. Zhang, A. H. Macdonald, and R. S. Ruoff, *Nat. Commun.*, 2014, **5**, 3317.

[20]   J. Xia, F. Chen, J. Li, and N. Tao, *Nat. Nanotechnol.*, 2009, **4**, 505.

Nanoscale Accepted Manuscript